

# Self-assembly of peptide-based nanostructures: Synthesis and biological activity

Léna Guyon, Elise Lepeltier (✉), and Catherine Passirani

Micro & Nanomédecines Translationnelles-MINT, UNIV Angers, INSERM U1066, CNRS UMR 6021, UBL Université Bretagne Loire, Angers F-49933, France

**Received:** 8 March 2017  
**Revised:** 20 October 2017  
**Accepted:** 21 October 2017

© Tsinghua University Press  
and Springer-Verlag GmbH  
Germany 2017

## KEYWORDS

self-assembly,  
cell penetrating peptide,  
nanoparticle,  
peptide

## ABSTRACT

Peptide-based nanostructures have received much attention in the field of drug targeting. In fact, peptides have many advantages such as simplicity of the structure, biocompatibility, and chemical diversity. Moreover, some peptides, which are called cell-penetrating peptides, can cross cellular membranes and carry small molecules, small interfering RNA, or viruses inside live cells. These molecules are often covalently or noncovalently linked to cargoes, thus forming amphiphilic conjugates that can self-assemble. Supramolecular nanostructures formed from peptides are used in nanomedicine as a carrier to protect a drug and to target cancer cells. This review explores aliphatic-chain-conjugated peptides and drug-conjugated peptides that can self-assemble. Special emphasis is placed on the synthesis procedure, nanostructure formation, and biological activity.

## 1 Introduction

One strategy to obtain nanoparticles is to apply knowledge learned from natural biological systems to building of supramolecular structures, formed by intermolecular forces such as hydrogen bonds (H-bonds), van der Waals forces, and hydrophobic interactions. These interactions can lead to various structures such as dendrimers, micelles, liposomes, or lipid nanocapsules (Fig. 1). Initial research efforts were focused on encapsulating drugs to minimize their degradation and increase drug bioavailability and accumulation at a target site. Historically, the first practical systems were liposomes, discovered in 1965

[1, 2], and micellar formulations [3, 4]. Liposomes can be obtained by hydration of a thin lipid film; the self-assembly of lipids leads to bilayers mimicking a cell membrane [5, 6]. This system has the ability to carry hydrophobic and amphiphilic compounds as cargo in the lipid bilayer and/or hydrophilic molecules in the aqueous internal cavity [7].

Prediction of the structure of a self-assembled object has been the focus of numerous studies [8–15]. An original approach was developed by Israelachvili to predict the supramolecular structures of self-assembled amphiphilic molecules in water [12–15]. Indeed, the study of the supramolecular organization of a nano-assembly is essential for therapeutic purposes; the

Address correspondence to [elise.lepeltier@univ-angers.fr](mailto:elise.lepeltier@univ-angers.fr)

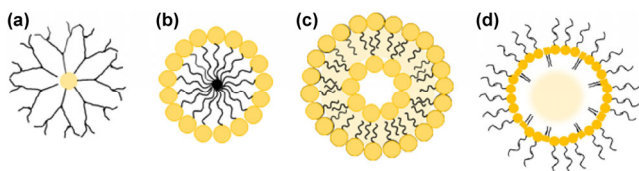


**Figure 1** Schematic presentation of dendrimers (a), micelles (b), liposomes (c) and lipid nanocapsules (d).

structure has an influence on the biological activity of the self-assembly if different parameters are varied by researchers, e.g., stability in biological media, the ability to diffuse through tissues, and internalization by cells [16].

The use of natural building blocks such as phospholipids, oligosaccharides, oligonucleotides, proteins, and peptides has attracted much attention regarding the fabrication of new materials [17–21]. Among all these building blocks, peptides have aroused tremendous interest owing to their simple structure, biocompatibility or biodegradability, and chemical diversity.

In this review, different strategies to design peptide-based conjugates that can self-assemble are discussed. Particular emphasis is placed on i) aliphatic-chain-conjugated peptides and ii) drug-conjugated peptides. For each topic, the synthesis procedure, nanostructure formation, and biological activity will be overviewed.

## 2 Aliphatic-chain-conjugated peptides

This section provides an overview of aliphatic-chain-conjugated peptides that have the ability to self-assemble. The focus is on amphiphilic peptides with biological applications. First, the synthesis of the amphiphilic compounds is examined, followed by an overview of the self-assembly procedure and a description of the structure obtained. Finally, biological-activity studies are reported.

### 2.1 Preparation of amphiphilic compounds

A member of the class of peptide amphiphiles (PAs) consists of a hydrophilic peptide sequence attached to hydrophobic lipid chains through an amide bond. Peptides are biomolecules that have unique chemical and physical properties as a function of their primary structure (amino acid composition), secondary structure

( $\alpha$ -helix and  $\beta$ -sheet) and three-dimensional or tertiary structure. Thus, different peptides are used in a wide range of applications.

In most studies, peptides are prepared by solid-phase peptide synthesis using standard 9-fluorenylmethoxycarbonyl (Fmoc) chemistry. After this step, two approaches are considered:

- 1) The aliphatic chain is linked using the same strategy (solid-phase synthesis) [22–33].
- 2) The aliphatic chain is linked via chemical reactions after cleavage of the peptide from the resin [34, 35].

#### 2.1.1 Aliphatic-chain-coupling reaction on the resin

Zongguang Tai et al. applied the first approach [22, 23]. In their studies, the peptide  $H_3CR_5C$  was synthesized on the resin and then the stearyl moiety was attached to the N-terminal extremity of the peptide [22, 23]. Thus, the total synthesis was conducted on the resin, allowing for simplification of the purification step. More often, the conjugates were cleaved from the resin by means of a mixture containing trifluoroacetic acid and purified by preparative reverse-phase high-performance liquid chromatography (RP-HPLC). Nonetheless, a correlation was found between the length of the chain and difficulty of the coupling. In fact, the reaction with a fatty acid containing six carbon atoms was successful after at least 6 h of incubation [24].

#### 2.1.2 Aliphatic-chain-coupling reaction after cleavage

In the second approach, the aliphatic chain needs to be functionalized to react with the peptide. Tang Q. et al. modified cholesterol with acryloyl chloride to obtain cholesterol acrylate, and then they conjugated it with peptides containing a C-terminal cysteine residue through a thiol-acrylate Michael-type reaction, under slightly basic conditions [34]. Using this strategy, those authors synthesized four conjugates containing different peptide sequences:  $Ch-CH_5R_5$ ,  $Ch-CH_3R_3$ ,  $Ch-CR_5$  and  $Ch-CR_3$  (structures are shown in Fig. 2).

Peters D. et al. used the thiol group of cysteine-containing peptides for covalent conjugation to the lipid tail. In fact, DSPE-PEG<sub>2000</sub>-maleimide was conjugated to the peptide via a thioether linkage [36].

Another way is to obtain an alkyne-modified lipid and an azide-modified peptide [35]. These modifications allow investigators to link the peptide and lipid via

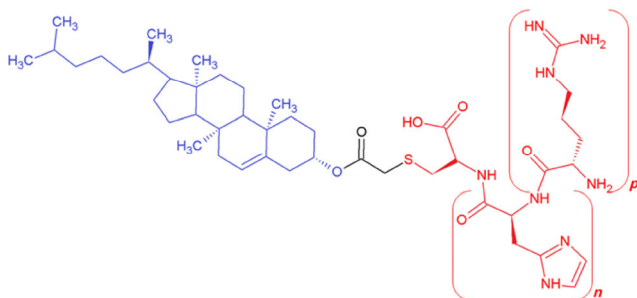


**Figure 2** Chemical structure of cholesterol-peptide conjugates Ch-Cys-His<sub>n</sub>-Arg<sub>p</sub> with  $n = 0, 3, 5$  and  $p = 3, 5$ . Cholesterol represented in blue and peptide in red.

a click reaction [37]. With this objective in mind, T. Matsubara et al. synthesized a peptide with an azide group through the side chain of Lys (ARLPRK(N<sub>3</sub>)-NH<sub>2</sub>) according to the Fmoc strategy. To prepare an alkyne-containing lipid, those authors modified the lipid (dipalmitoylphosphatidylethanolamine; DPPE) with 4-pentynoic acid to obtain N-(4-pentynoyl)-DPPE (Fig. 3). After these two steps, the coupling of pentynoyl-DPPE with azide-peptide was performed.

## 2.2 Nanostructures formed by self-assembly

### 2.2.1 Nanofibers

A number of PA molecules have been demonstrated to self-assemble into cylindrical nanofibers, as a result of H-bonding among peptide segments and hydrophobic collapse of alkyl tails [24, 32, 38, 39]. These cylindrical structures were obtained in aqueous media in the presence of suitable stimuli for example, pH induction of self-assembly [24, 40]. Honggang Cui et al. showed that an alkyl segment with 16 carbons (palmitic acid) grafted to a tetrapeptide sequence, containing hydrophobic and negatively charged residues (Val-Glu-Val-Glu), self-assembled into nanobelts in an

aqueous solution at a concentration of 0.1 wt.% [40]. The nanobelts obtained had relatively monodisperse width on the order of 150 nm and length of up to 0.1 mm according to atomic force microscopy (AFM) experiments.

The influence of the self-assembly formulation on the resulting nanostructures is of interest. In this regard, Jeffrey D. Hartgerink et al. described two different modes of self-assembly [24]: Acid-induced self-assembly and divalent-ion induction. For the acid-induced self-assembly, those authors obtain nanofibers with a PA, such as C<sub>16</sub>H<sub>31</sub>O grafted to C<sub>4</sub>G<sub>3</sub>S(PO<sub>4</sub>)RGD, dissolved in water and exposed to HCl vapor. They showed as well that treatment of a solution of these conjugates with Ca<sup>2+</sup> instantly resulted in gelation of the solution. For this purpose, CaCl<sub>2</sub> was dropwise added to a solution of a PA. After transmission electron microscopy (TEM) examination, it was found that the gel was comprised of nanofibers with the same dimensions as those resulting from acid-induced self-assembly. Thus, nanofibers were obtained with a diameter between 5 and 8 nm; the length and stiffness of the formed fibers depended on the peptide used. This Ca<sup>2+</sup>-induced self-assembly may be particularly helpful for medical applications, where formation of a gel at physiological pH is required [24]. Similarly, PA filaments that are designed to mimic the activity of the vascular endothelial growth factor (VEGF) peptide can form a gel network at low concentrations in aqueous media [32]. In that study, Webber M. J. et al. developed a cell-free therapy based on PA nanostructures for ischemic heart disease. To this end, the K<sub>3</sub>G peptide was covalently linked to the N-terminal extremity of a VEGF-mimetic peptide to increase water solubility, and the C<sub>16</sub>-V<sub>2</sub>A<sub>2</sub> tail was added

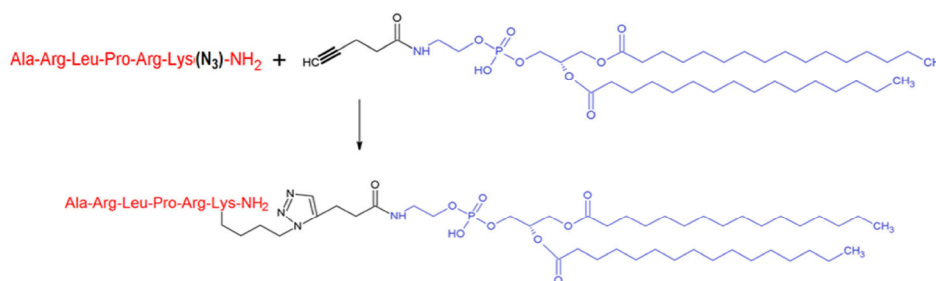


**Figure 3** Synthesis of peptide-DPPE conjugates via the click reaction of pentynoyl-DPPE and an azide containing a pentapeptide (adapted with permission from Ref. [35], © Front. Microbiol. 2016).

to facilitate self-assembly into cylindrical structures. Accordingly, the following sequence was formed: C<sub>16</sub>-V<sub>2</sub>A<sub>2</sub>K<sub>3</sub>GKLTWQELYQLKYKGI (VEGF PA). The analysis of this PA by TEM experiments revealed formation of cylindrical nanostructures that caused congealing in the presence of divalent counterions (Na<sub>2</sub>HPO<sub>4</sub>; Fig. 4).

Furthermore, hydrogelation of four PAs was studied by Matson J. B. et al. with regard to drug delivery applications [39]. Figure 5 shows the chemical structure of a PA molecule (C<sub>16</sub>V<sub>2</sub>A<sub>2</sub>E<sub>2</sub>) developed by the Stupp group, and this PA has three key structural features. This peptide sequence, C<sub>16</sub>V<sub>2</sub>A<sub>2</sub>E<sub>2</sub>, which contains a derivatized hydrazide has been investigated, and prodan, which is typically used as a dielectric probe for cell membranes, served as a model molecule. To control the drug release, prodan was linked to the peptide through a hydrazine bond at a different position along the backbone of the peptide. This pH-sensitive bond can be destroyed in the acidic environment of a cell compartment. Hydrogel formation was induced by adding a 100 mM CaCl<sub>2</sub> solution after dissolving PA in NaOH. After small angle X-ray scattering examination, it was shown that the cross-sectional diameter of the gel depended on lysine-hydrazide-prodan residue position; the largest diameter was obtained with C<sub>16</sub>V<sub>2</sub>A<sub>2</sub>E<sub>2</sub>K(Hyd-Prodan) (10.8 nm), C<sub>16</sub>V<sub>2</sub>A<sub>2</sub>K(Hyd-Prodan)E<sub>2</sub>, and C<sub>16</sub>V<sub>2</sub>K(Hyd-Prodan)A<sub>2</sub>E<sub>2</sub> had the same diameter (10.5 nm), whereas C<sub>16</sub>K(Hyd-Prodan)V<sub>2</sub>A<sub>2</sub>E<sub>2</sub> had the smallest size (10.4 nm; Fig. 6).

### 2.2.2 Micelles

The same amphiphilic conjugates, with the same chemical structure, can be applied to creation of a

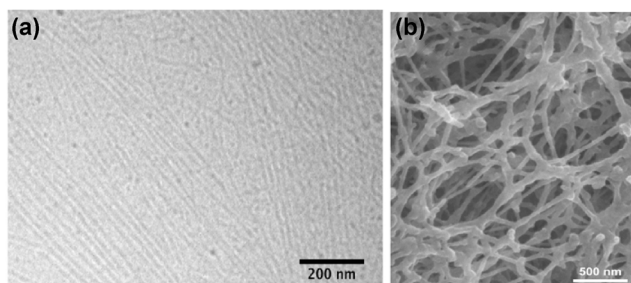


**Figure 4** TEM image of nanofibers obtained with VEGF PA and SEM image of entangled nanofiber gel formed (reprinted with permission from Ref. [32], © National Academy of Sciences 2011).

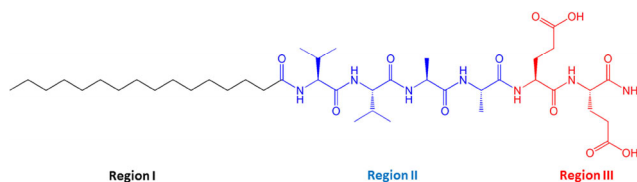


**Figure 5** Chemical structure of a representative PA C<sub>16</sub>V<sub>2</sub>A<sub>2</sub>E<sub>2</sub> which is composed of three entities. Region I, hydrophobic tail; region II:  $\beta$ -sheet forming segment; region III, charged groups.

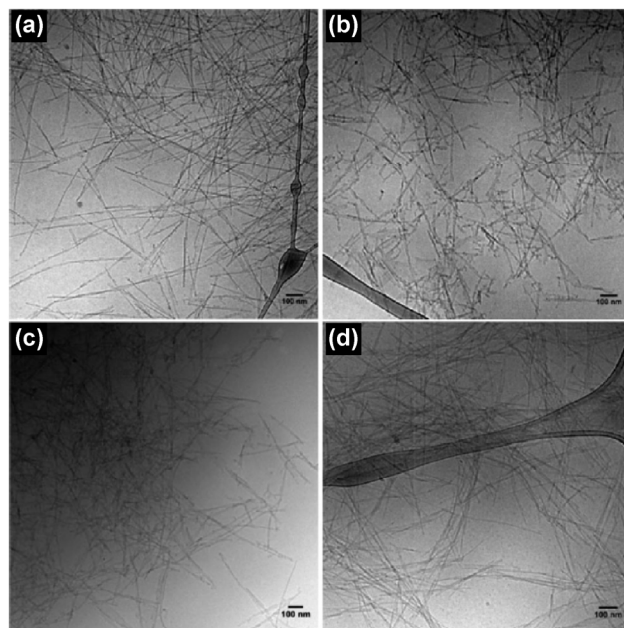


**Figure 6** TEM images of (a) C<sub>16</sub>V<sub>2</sub>A<sub>2</sub>E<sub>2</sub>K(Hyd-Prodan), (b) C<sub>16</sub>V<sub>2</sub>A<sub>2</sub>K(Hyd-Prodan)E<sub>2</sub>, (c) C<sub>16</sub>V<sub>2</sub>K(Hyd-Prodan)A<sub>2</sub>E<sub>2</sub>, (d) C<sub>16</sub>K(Hyd-Prodan)V<sub>2</sub>A<sub>2</sub>E<sub>2</sub> (reprinted with permission from Ref. [39], © American Chemical Society 2012).

different self-assembled nanostructure (Fig. 7). In fact, stearyl-H<sub>3</sub>CR<sub>5</sub>C conjugates that are crosslinked by disulfide bond (SHR<sub>2</sub>S) have been used to form doxorubicin (DOX)-loaded micelles by nanoprecipitation and probe-based ultrasonication methods. The micelles formed by self-assembly are comprised of a hydrophilic shell and a hydrophobic core with an average diameter of 233 nm. DOX is then loaded into the micelles through hydrophobic interactions [22]. On the other hand, stearyl-peptide conjugates may effectively condense small interfering RNA (siRNA) into polyplexes with a hydrodynamic size of 100–300 nm [23]. In both cases, the same principle is followed for self-assembly, based on the nanoprecipitation technique.

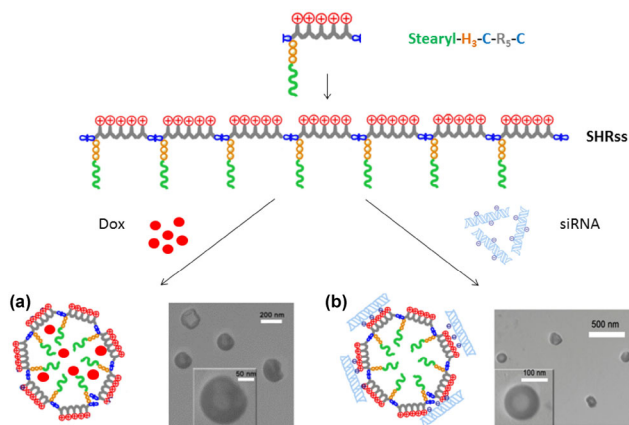


**Figure 7** Nanostructures obtained with disulfide cross-linked SHRs. (a) Doxorubicin loaded micelles and (b) nanoparticles with negatively charged siRNA (adapted with permission from Ref. [22], © Elsevier B.V. 2016 and Ref. [23], © Elsevier B.V. 2015).

In the first case, a solution of DOX·HCl in dichloromethane is injected dropwise into the peptide solution followed by ultrasonication and evaporation of the solvent. In the second case, the peptides are complexed with siRNA in phosphate-buffered saline (PBS, 50  $\mu$ L per 0.5  $\mu$ g of siRNA at pH 6.0), and the sample is vortexed.

Four amphiphilic cholesterol-peptide conjugates (Ch-CH<sub>5</sub>R<sub>5</sub>, Ch-CH<sub>3</sub>R<sub>3</sub>, Ch-CR<sub>5</sub>, and Ch-CR<sub>3</sub>, structures are shown in Fig. 2) can also self-assemble into cationic micelles at low concentrations in PBS [34]. In that study, the cholesterol-peptide–DNA complexes were formed by mixing equal volumes of cholesterol-peptide in PBS (at 10 mg·mL<sup>-1</sup>) and DNA in nuclease-free water (at 1 mg·mL<sup>-1</sup>). Those authors showed that the size of the obtained complexes with DNA depended on the *R/P* ratio (molar ratio of arginine residues (*R*) in the peptide to phosphate groups (*P*) in the DNA molecule). For example, for Ch-CH<sub>5</sub>R<sub>5</sub>, the size was 718 nm at the *R/P* ratio of 5 and decreased as the *R/P* ratio increased from 10 to 30. Therefore, the smallest complexes were obtained at the *R/P* ratio of 30 with a size of 179 nm.

Formation of micelles with palmitoyl-p53<sub>14-29</sub> has been studied by D. Missirlis et al. [28]. This PA self-assembled in 10 mM phosphate buffer; the hydrophobic interactions induced formation of micelles with a hydrodynamic diameter of 319 nm but also elongated micelles with a diameter of 10 nm and a length of few

hundred nanometers. Another method for preparation of micelles involves film casting by dissolving PA in an organic solvent such as methanol or chloroform and by evaporating the solvent under an inert gas. Micelle formation proceeds after hydration of the film with water or phosphate buffer followed by a vortexing step [29]. This method was used by A. Trent et al. to construct J<sub>8</sub>-diC<sub>16</sub> micelles comprised of the J8 peptide (QAEDKVKQSREAKKQVEKALKQLEDKVKQK) and a hydrophobic moiety: Dipalmitoylglutamic acid (diC<sub>16</sub>). TEM analysis revealed the formation of cylindrical micelles 5–15 nm in diameter and 25–125 nm in length (Fig. 8). These nanostructures were studied as a self-adjutant for the development of group A streptococcal (GAS) vaccines to increase an injectable-peptide concentration and protect the peptide from degradation [41].

### 2.2.3 Lipid bilayer

It could be pointed out that, as a supramolecular structure of aliphatic-chain-conjugated peptide self-assemblies, nanofibers and micelles are obtained mainly. Nevertheless, a lipid bilayer may be constructed under certain conditions. Matsubara T. and coworkers described preparation of a lipid bilayer on a mica plate. A POPC (1-palmitoyl-2-oleoyl-sn-glycero-3-phosphocholine) lipid monolayer at the air–water interface was prepared by the Langmuir–Blodgett technology and transferred to a freshly cleaved mica plate by horizontal deposition. Then, a second lipid monolayer of a peptide-conjugated lipid (structure shown in Fig. 9) was loaded onto the POPC-coated mica [35, 42, 43]. The Langmuir–Blodgett

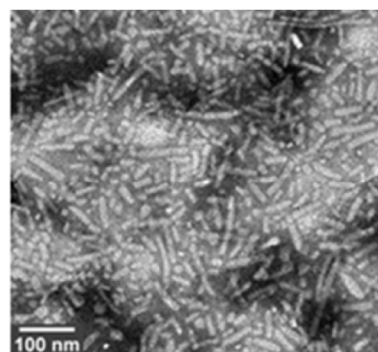


**Figure 8** TEM images of cylindrical micelles obtained with J<sub>8</sub>-diC<sub>16</sub> (reprinted with permission from Ref. [41], © Springer 2014).

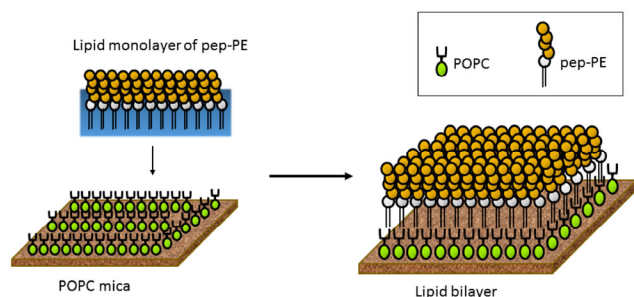


**Figure 9** Procedure of construction of pep-PE lipid membrane. A pep-PE monolayer was transferred to the POPC-coated mica to give the pep-PE lipid bilayer (adapted with permission from Ref. [35], © Front. Microbiol. 2016).

deposition was also used with different PAs of the following sequences:  $(C_{18})_2$ -E-C<sub>2</sub>-RGD (amino-coupled tripeptide RGD), RGD-C<sub>2</sub>-E- $(C_{18})_2$  (carboxyl-coupled RGD), and  $(C_{18})_2$ -E-C<sub>2</sub>-RGD-C<sub>2</sub>-E- $(C_{18})_2$  (lopped RGD). Those authors obtained monolayers that can act as biomimetic membranes that present a uniformly oriented peptide sequence to the cell [44].

### 2.3 *In vitro* and *in vivo* studies

Self-assembled PAs possess several attractive features for different applications, and many studies are focused on drug or gene therapy in the context of cancer treatment but also on tissue regeneration. This subsection is not an exhaustive selection of biological studies covering various applications.

#### 2.3.1 *Cancer treatment*

DOX-loaded micelles formed from stearyl- $H_3CR_5C$  have been studied in the context of androgen-independent prostate cancer cells [22]. Experiments have been carried out to study some properties of these complexes, such as an *in vitro* drug release. During these experiments, performed in a dialysis bag (molecular weight cutoff 3,500 Da) immersed in PBS containing Tween 80 and GSH (glutathione is a tripeptide used to mimic the cell environment and reduce disulfide bonds), the concentration of the released DOX was quantified by means of a UV spectrometer at selected time intervals. The obtained DOX release profiles showed a strong pH influence (Fig. 10). In fact, a larger amount of drugs was released at pH 5.5 (82.6%) than at pH 7.4 (63.3%). The *in vitro* release behaviors of DOX-loaded micelles suggest that

DOX is released faster at endolysosomal pH than at physiological pH. Cellular uptake has also been investigated by flow cytometry (fluorescence-activated cell sorting) and confocal laser scanning microscopy (CLSM) on DU145 cells (a human prostate cancer cell line). As shown in Fig. 11, DOX was detected in the nuclear and perinuclear regions of the cytoplasm after 1 h of incubation. Moreover, the results indicated that the uptake of micelles was time-dependent with an intracellular uptake rate higher after 4 h of incubation ( $89.50 \pm 0.99\%$ ) than after 1-h incubation ( $82.56 \pm 1.55\%$ ). It can be concluded that this amphiphilic micellar system stimulates the chemotherapeutic drug

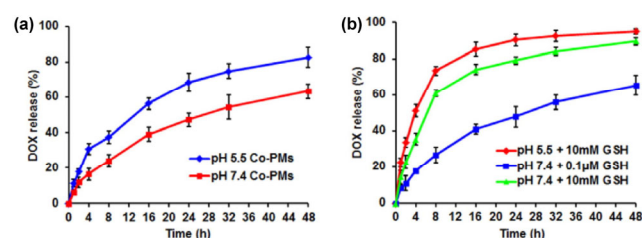


**Figure 10** Dox release profiles of Co-PMs. (a) In PBS at pH 5.5 and 7.4, (b) with the presence of GSH in PBS at pH 5.5 and 7.4 (reprinted with permission from Ref. [22], © Elsevier B.V. 2016).

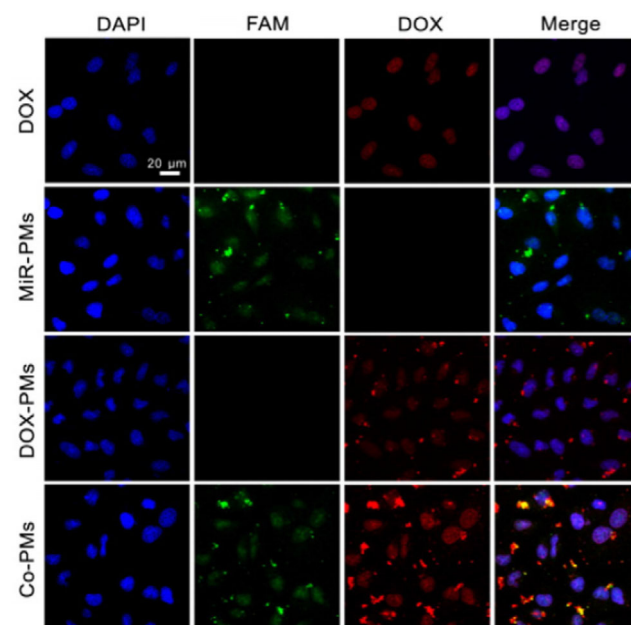


**Figure 11** Confocal microscopy images. Images of DU145 cells after incubation with DOX, MiR-PMs, DOX-PMs and Co-PMs for 1 h (reprinted with permission from Ref. [22], © Elsevier B.V. 2016).

release into the cell nucleus, thereby improving the antitumor activity of DOX via the downregulation of SiRT1 and by reducing the cardiotoxicity of DOX.

### 2.3.2 Gene therapy

Stearyl peptides can also serve as a delivery carrier of siRNA [23]. Tai, Z. G. et al. compared the cellular uptake of disulfide bond-linked stearyl-H<sub>3</sub>CR<sub>5</sub>C (SHRss) by means of Lipofectamine 2000 (LF2000), which is a common transfection agent helping to increase the efficiency of transfection of RNA. Flow-cytometric analysis revealed that the cellular uptake efficiency of SHRss was much higher than that of LF2000 in Luc-HeLa cells (a human cervical cancer cell line; Fig. 12). The siRNA silencing efficiency was also evaluated in Luc-HeLa cells and mCherry-HEK293 cells (human embryonic kidney cells that express red fluorescent protein) as reporter cell lines. Experiments indicated that introduction of a disulfide bond between stearyl-H<sub>3</sub>CR<sub>5</sub>C and XYZ enabled significantly stronger gene silencing. CLSM analysis was also performed and showed the ability of SHRss–siRNA complexes to enhance cellular uptake and release siRNA into the cytoplasm. As for cytotoxicity, SHRss–siRNA complexes yielded higher cell viability than LF2000 did. Moreover, the results indicated that bioreducible disulfide bonds may decrease toxicity and improve biocompatibility. Furthermore, the *in vivo* studies showed that SHRss–siRNA complexes have high efficacy of RNA interference (gene knockdown).

Another system, the one comprised of cholesterol-conjugated peptides, has been investigated as a gene delivery carrier [34]. The DNA-binding ability of

cholesterol-peptides was assessed by an agarose gel retardation assay and the results suggested that the highest DNA-binding ability belongs to the Ch-R<sub>5</sub>H<sub>5</sub> conjugate. After that, the luciferase expression enhancement by complexes of a cholesterol-peptide with DNA was quantified. This experiment revealed that the cholesterol-peptide conjugate with histidine residues yielded higher luciferase expression than the conjugates without histidine. This result was due to the buffering capacity of histidine, which facilitated DNA escape from endosomes. Elongated PA wormlike micelles formed from palmitoyl-p53<sub>14-29</sub> have been studied on SJS-1 osteosarcoma cells.

### 2.3.3 Bone and tissue regeneration

The formation of PA gels has been studied for various biological applications such as bone and tissue regeneration [25, 26]. Mata et al. evaluated the bone regeneration potential of a PA in a nonhealing rat femoral defect. The results showed successful formation of biomimetic bone crystals and enhancement of bone regeneration owing to phosphorylated serine residues contained in supramolecular nanofibers [25]. Cell entrapment in PA gels was also evaluated for cell transplantation and other tissue-engineering applications [38]. According to optical micrographs of MC<sub>3</sub>T<sub>3</sub>-E1 cells (mouse osteoblastic cell line) entrapped in KGE PA gels, the cells adopted a spindle-like shape immediately after entrapment. Moreover, TEM analysis suggested that cells internalized the nanofiber by endocytosis, indicating that nanofibers can be degraded by natural mechanisms without any cytotoxicity. Control of a drug release was assessed by J. B. Matson

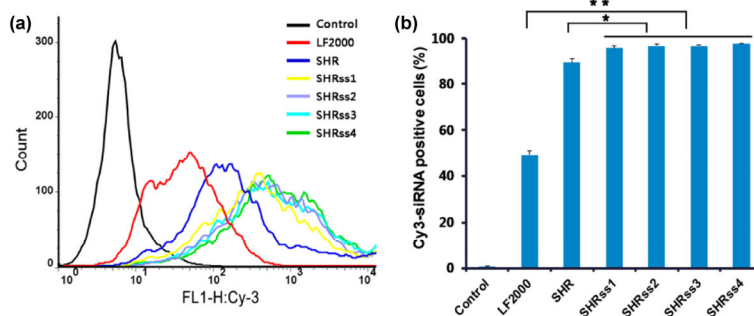


**Figure 12** Flow cytometry of SHRss/Cy3-siRNA uptake. Cellular uptake analysis of various Cy3-siRNA complexes ( $N/P = 10$ ) (a) and the ratio of Cy3-siRNA positive cells (b) after 3 h transfection in Luc-Hela cells (final Cy3-siRNA concentration, 75 nM). The untreated cells were used as the control. Reprinted with permission from Ref. [23], © American Chemical Society 2015.

et al. on filamentous gels comprised of  $C_{16}V_2A_2E_2$  and prodan attached at different positions along the backbone of the PA. The release of prodan from the hydrogel, which requires hydrazone hydrolysis and diffusion from the gel, was studied at physiological pH in phosphate buffer. Fluorescence measurements revealed that a gel formed from  $C_{16}K(\text{Hyd-Prodan})V_2A_2E_2$  PA yielded the fastest hydrolysis. Moreover, circular dichroism experiments showed that the distance between the lysine branch and the alkyl tail had an impact on the properties of the nanostructures. In fact, the lysine-hydrazone-prodan tail position determined packing density, which can regulate the mobility of prodan and the accessibility of hydrazine to the solvent. That study highlights the importance of the formed supramolecular structure for control over a drug release for regenerative-medicine applications [39].

#### 2.3.4 Ischemia treatment

Webber, M. J. et al. designed nanostructures that can mimic the activity of VEGF for therapeutic angiogenesis. Biological activity of the PA nanostructure was investigated *in vitro* in human umbilical vein endothelial cells. Phosphorylation assays indicated that VEGF PA specifically activated VEGF receptors as compared to no-treatment control. For *in vivo* testing, those authors carried out a chicken chorioallantoic membrane assay to estimate the angiogenic activity of the VEGF PA. After 3 days of treatment, they detected a 229% increase in the blood vessel density, thus confirming the proangiogenic properties of this PA. Evaluation of therapeutic properties of these VEGF PA nanostructures in a murine hind-limb ischemia model revealed the potential of this system to restore perfusion in ischemic tissue [32].

#### 2.3.5 Detection of influenza virus

Peptide-conjugated lipids have also been studied as a molecular device for the detection of hemagglutinin (HA), which is a glycoprotein responsible for binding of the influenza virus to the plasma membrane via sialic acid residues [35]. Those authors developed a peptide-conjugated lipid that can fully replace gangliosides in the cell membrane. A sialic-acid-mimicking pentapeptide was conjugated to DPPE

and tested as a constituent of the lipid bilayers, which were immobilized on a mica slice. To study the binding of influenza HA, the surface topography of the obtained membrane was then analyzed by AFM. The results indicated that HA preferentially bound to the sialic-acid-mimicking peptide. In fact, they observed no significant binding to the free DPPE membrane. This peptide-conjugated lipid membrane manifested useful affinity for HA and influenza virus, thereby facilitating the diagnosis and surveillance of influenza or other sugar-related diseases.

#### 2.3.6 Biomimetic coating

The biological activity of looped RGD monolayers as biomimetic coating has been investigated. The metastatic human melanoma cell line (M14#5) was used for *in vitro* testing to evaluate the cell spreading response on films. Results showed that the spatial orientation and molar concentration of the PA were crucial for determination of their ability to promote and prevent cellular response. The treatment of cells with anti-integrin receptor monoclonal antibodies suggested that the PA holds promise for control of cellular behavior via specific receptor-ligand interactions [44].

## 3 Drug-conjugated peptides

Several drugs have been conjugated to different peptides to enhance the cellular uptake and retention of the drug. Moreover, a covalent linkage of drugs to a carrier can improve drug solubility and specificity [45]. In this subsection, we present the most widely studied peptide-drug conjugates that are able to self-assemble. This subsection is organized by function of the drug under study: DOX, paclitaxel, and camptothecin (CPT). For each platform, the synthesis procedure, analysis of the nanostructures formed, and biological activity is discussed.

### 3.1 DOX-conjugated peptides

#### 3.1.1 Preparation of amphiphilic compounds

DOX is a chemotherapeutic agent for the treatment of cancers, including hematopoietic cancers; carcinomas of the breast, lung, ovary, and stomach; and soft tissue



sarcomas [46]. To maximize the therapeutic index, DOX is linked to a macromolecular drug carrier.

In the case of DOX, three peptide types commonly serve as macromolecular carriers to enhance drug delivery of DOX: Elastin-like polypeptides (ELPs), chimeric polypeptides (CPs), and cell-penetrating peptides (CPPs).

When ELPs are used as a macromolecular carrier, the first step is the synthesis of a recombinant ELP. After this step, the ELP is either functionalized or coupled directly via a maleimide/thiol reaction with a lysine residue. For the first method, the ELP is modified with SMCC (succinimidyl 4-(N-maleimidomethyl)cyclohexane-1-carboxylate) to provide a maleimide moiety. DOX hydrochloride is modified with a hydrazone linker that contains a disulfide bond. Finally, ELP-maleimide is reacted with DOX-hydrazone in the presence of Tris(2-carboxyethyl)phosphine, enabling reduction of the disulfide bond (Fig. 13) [47].

In the second method, DOX reacts with  $n$ - $\beta$ -maleimidopropionic acid hydrazide, thereby incorporating an internal, acid-labile hydrazone moiety with a terminal maleimide. Next, the maleimide moiety reacts with the thiol group of the lysine residue of the ELP [48].

Via the same strategy, the chimeric polypeptide SKGPG(XGVPG)<sub>160</sub>WPC(GGC)<sub>8</sub> is conjugated to DOX. The polypeptide segment provides eight drug attachment points via the cysteine residue, as shown in Fig. 14.

Concerning the procedure steps, CP is first synthesized by a recombinant method from a plasmid-borne synthetic gene in *E. coli*. After that, DOX is functionalized

with a hydrazone moiety, which contains a terminal maleimide. The next step is the click reaction between the thiol of CP and the maleimide of functionalized DOX [49, 50].

Cheng, H. et al. described conjugation of an activable cell-penetrating peptide (CR<sub>8</sub>G<sub>3</sub>PK<sub>6</sub>, ACPP), which contained a shielding group of 2,3-dimethylmaleic anhydride (DMA), with DOX. The conjugate synthesis was divided into four steps. First, the peptide synthesis was performed manually by a standard Fmoc solid-phase peptide synthesis method. Then, DOX was functionalized with N-succinimidyl 3-maleimidopropionate (SMP). The third step was the DOX-SMP-ACPP synthesis via a Michael addition reaction between thiol and maleimide. Finally, DMA was linked to ACPP to obtain DOX-ACPP-DMA, for inhibition of the cell-penetrating function of the octa-arginine at physiological pH through intramolecular electrostatic attraction [51]. Peptide-DOX conjugates are often synthesized by coupling a peptide with DOX via a linker of SMP [51–53]. Another popular cross-linker is SMCC. It is used, for example, to conjugate DOX with the Tat peptide (CGGGYGRKKRRQRRR) [54].

In both cases, the strategy for the conjugation is a thiol-maleimide “click” chemistry reaction.

### 3.1.2 Nanostructures formed by self-assembly

Nanoparticles and especially micelles are mainly constructed from peptide-DOX conjugates to decrease the high cytotoxicity and improve the selectivity of DOX. In general, such nanostructures are obtained by spontaneous self-assembly in PBS. In this regard, Dreher et al. conjugated DOX to an ELP through an

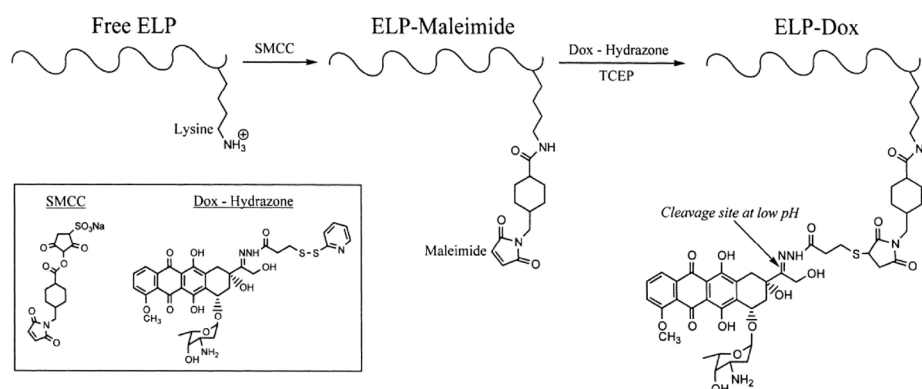


**Figure 13** Conjugation scheme for doxorubicin ELP conjugate (reprinted with permission from Ref. [47], © American Chemical Society 2003).

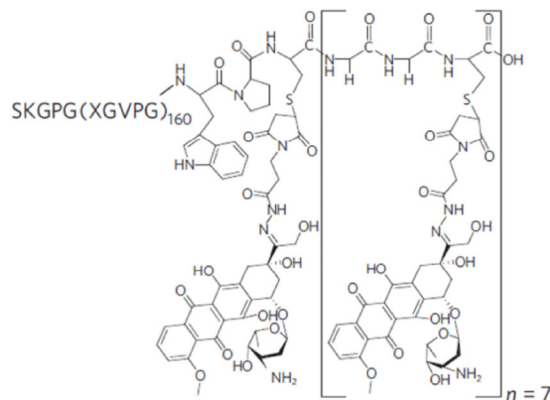


**Figure 14** Chemical structure of chimeric polypeptide-DOX conjugate (reprinted with permission from Ref. [49], © American Chemical Society 2015).

acid-labile hydrazine bond. Self-assembly of these conjugates was temperature-dependent; ELP-DOX formed micelle structures below its first phase transition ( $T = 39.66\text{ }^{\circ}\text{C}$  at a concentration of 13.3 mM) with an average hydrodynamic radius of 21 nm and a terminal aggregate after its transition temperature [47]. Similarly, upon conjugation to DOX, a chimeric polypeptide comprised of a hydrophilic ELP and a C-terminal C(GGC)<sub>7</sub> peptide segment self-assembled into micelles of 40-nm diameter, according to AFM and dynamic light scattering (DLS) assays [49, 50].

In other cases, self-assembly can be applied to inhibit the cell-penetrating function. Tsien's group conjugated an ACPD to DOX and to a shielding group of DMA, to form DOX-ACPD-DMA conjugates. Consequently, self-assembly, monitored by electrostatic attraction between octa-arginine ( $R_8$ ) and polylysine, could be used to block the cell-penetrating function of octa-arginine (Fig. 15) [51, 52].

### 3.1.3 Biological activity

An ELP-DOX conjugate was tested on squamous cell

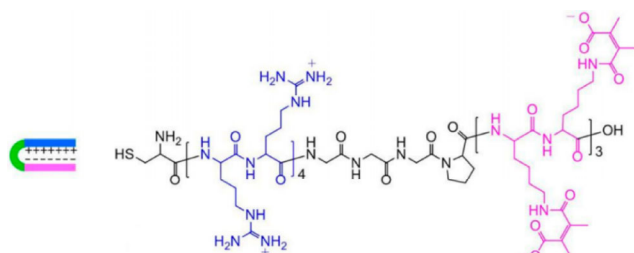


**Figure 15** Structure of DOX-ACPD-DMA (reprinted with permission from Ref. [51], © American Chemical Society 2015).

carcinoma (FaDu cells) [47]. The conjugation of an ELP to DOX was achieved through an acid-labile hydrazone bond to promote the release of DOX from the ELP at low pH ( $\text{pH} \approx 5$ ). The cytotoxicity analysis of the ELP-DOX conjugate showed cytotoxicity comparable to that of free DOX (Fig. 16).

Besides, the cellular localization of DOX and ELP-DOX has been evaluated to compare the mechanisms of cytotoxicity. In the form of the conjugate, DOX was mostly concentrated in the cytoplasm. On the contrary, free DOX accumulated in the cell nucleus. To further investigate the intracellular localization, those authors utilized Alexa 488, a green fluorescent dye with a molecular weight approximately equal to that of DOX, to label the ELP in order to study its cell distribution within FaDu cells. According to this experiment, internalized ELP and ELP-Alexa 488 were trafficked into lysosomes. Nevertheless, the hydrophobicity of DOX was greater than that of Alexa 488; this situation may result in a modification of the intracellular trafficking of the ELP [47]. By means of RP-HPLC, Darin, Y. et al. studied the pH-triggered release of DOX from an ELP-DOX conjugate by cleavage of the hydrazone bond. In that study, the ELP (SKGPG-ELP[(VPGXG)<sub>10</sub>]<sub>18</sub>-WPC) was linked to DOX via an aliphatic chain of various lengths. Those authors demonstrated that the spacer, and especially its hydrophobicity, affected the DOX release kinetics. In fact, the more hydrophobic the spacer, the smaller was the DOX release [48].

Intracellular localization of chimeric polypeptide SKGPG(XGVPG)<sub>160</sub>WPC(GGC)<sub>8</sub> conjugated to DOX

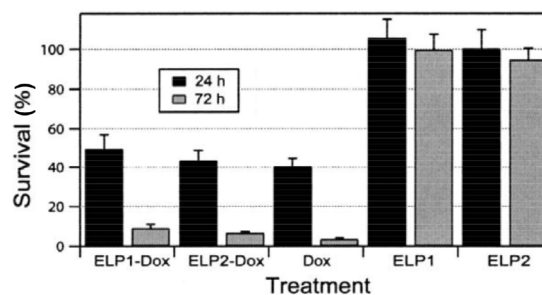


**Figure 16** Cytotoxicity of ELP1-dox (ELP1[V5A2G3-150]), ELP2-dox (ELP2 [V1A8G7-160]), doxorubicin, ELP1 and ELP2 against squamous cell carcinoma (FaDu) at 24 and 72 h post-treatment (reprinted with permission from Ref. [47], © Elsevier B.V. 2003).

(CP-DOX) has been studied in a murine colon carcinoma cell line (C26) [49]. To this end, the polypeptide was labeled with Oregon Green through a pH-insensitive thioether bond. According to the results obtained by laser scanning confocal fluorescence microscopy, CP was localized into endosomes and lysosomes. Moreover, the results showed slower uptake of CP-DOX compared with that of free DOX. The *in vivo* experiments performed on a mouse model suggested that nanoparticles accumulated in solid tumors, as the free drug did.

Furthermore, the maximum tolerated dose was higher for the CP-DOX nanoparticles. This result may be explained by an increase in tumor exposure and a decrease in heart exposure.

The same chimeric polypeptide (SKGPG(XGVPG)<sub>160</sub>WPC(GGC)<sub>8</sub>) conjugated with 4–6 DOX molecules has been studied by Mastria, E. M. et al. [50]. Free DOX and CP-DOX were injected at their respective maximum tolerated doses into mice that were inoculated with luciferase murine mammary carcinoma cells (4T1). According to the results, DOX conjugated with CP considerably prolonged blood plasma residence time and allowed to increase the DOX concentration within the plasma compartment. Those authors demonstrated the ability of the CP-DOX conjugate to inhibit metastasis of mammary 4T1 carcinoma (4T1) and Lewis lung carcinoma (LLC). For this purpose, mice were inoculated with 4T1-luc or LLC-luc and treated on days 8 and 15 postinoculation with free DOX or CP-DOX. During this experiment, metastasis and primary tumors were assessed two times per week by means of an IVIS Xenogen bioluminescent imaging system. The results revealed the ability of CP-DOX conjugates to inhibit metastasis and improve survival of the mice after a transplant of 4T1 and LLC syngeneic metastatic cell lines.

In addition, the use of an ACPP has been investigated as a carrier to translocate an antitumor drug into cells. To this end, an ACPP was conjugated with DOX but also to a shielding group (DMA) that could inhibit the activity of the ACPP at physiological pH. The antitumor effect of the DOX-ACPP-DMA conjugate was studied *in vitro* and *in vivo*. Evaluation of the enzymatic release of DOX was performed by dialysis in PBS. Cathepsin B, which is present in tumor cells,

enabled up to 70% of the DOX release within 10 h, because of the ability of this kind of protease to hydrolyze the amide bond. At the same time, CLSM analysis of the cellular uptake in HeLa cells (human cervical carcinoma cell line) was performed. After incubation from 6 to 24 h, the quantity of DOX in the cell nuclei increased, pointing to an effective release of DOX from the conjugate. *In vivo* experiments were performed on hepatic tumor cells (H22) in female KM mice. Those authors found that the xenograft tumor volume, during treatment with the DOX-ACPP-DMA conjugate, first increased slowly and then decreased sharply. Without any treatment, the tumor xenograft volume increased to 2,000 mm<sup>3</sup> after 14 days. By contrast, when the tumor was treated with DOX-ACPP-DMA, those authors observed a reduction in tumor volume to 50 mm<sup>3</sup> after 14 days, thereby demonstrating that DOX-ACPP-DMA considerably inhibited tumor growth [51].

Besides, ACPP-DOX has been used to develop a conjugate sensitive to matrix metalloproteinases (MMPs) for a tumor-targeting therapy [52]. Flow cytometry and CLSM analyses indicated that the cellular uptake of ACPP-DOX increased after enzyme-triggered activation and was higher in HT-1080 cells (human fibrosarcoma cells, overexpressing MMPs) than in MCF-7 cells (human breast adenocarcinoma cells, underexpressing MMPs).

## 3.2 Paclitaxel-conjugated peptides

### 3.2.1 Preparation of amphiphilic compounds

Paclitaxel, an anticancer agent that has potent antileukemic and tumor-inhibitory properties, was linked to peptides [55]. R. Tian et al. described the synthesis of a paclitaxel-CPP conjugate (Fig. 17). For this purpose, the CPP (EEGRLYMRYYSPTTTRYG) was first synthesized via standard Fmoc solid-phase peptide chemistry and was cleaved from the resin.

At the same time, the drug was functionalized with succinic anhydride (SA) to have a carboxylic acid function that can react with the N-terminal extremity of the CPP. Finally, paclitaxel-CPP was obtained through a carbodiimide-mediated coupling reaction between paclitaxel-SA-COOH and EEGRLYMRYYSPTTTRYG [56].

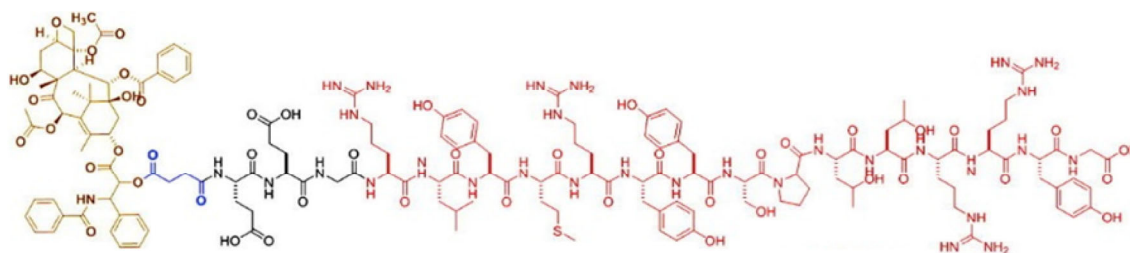


**Figure 17** Chemical structure of Paclitaxel-CPP conjugate (yellow extremity, paclitaxel; blue part, succinic acid; black part, tripeptide EEG; red chain, CPP) (reprinted with permission from Ref. [56], © Elsevier B.V. 2015).

It was also interesting to use a disulfide linker because its cleavage may occur only after cellular entry of the conjugate owing to the abundant presence of reduced glutathione (GSH). Dubikovskaya, E. A. et al. used this strategy to link paclitaxel to a peptide that contained a cysteine residue (Ac-NH-DCys-(DArg)<sub>8</sub>CONH<sub>2</sub>). To form a disulfide bond with paclitaxel, the drug was functionalized with 4-(pyridin-2-yl-disulfanyl)butyric acid. Then, a disulfide bond exchange reaction was carried out between thiol of the cysteine and the disulfide bond of the functionalized paclitaxel [57].

### 3.2.2 Nanostructures formed by self-assembly

Similarly to DOX, self-assembling structures with paclitaxel have been developed not only to control a drug release but also to improve water solubility. Self-assembly of peptide-paclitaxel conjugates can be achieved by directly dispersing the amphiphilic compound into distilled water or PBS (pH 7.4) during agitation. Tian, R. et al. developed supramolecular nanospheres of CPP-paclitaxel conjugates with an average diameter of ~ 120 nm (results obtained by TEM, shown in Fig. 18). According to DLS experiments, the

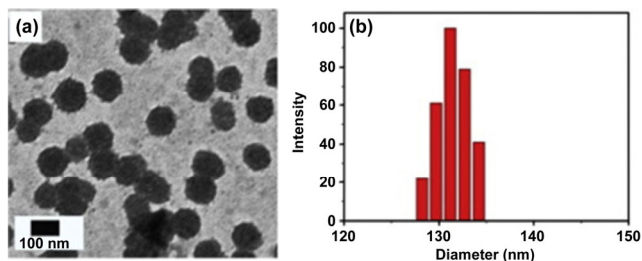


**Figure 18** (a) Negatively stained TEM image and (b) size distribution of paclitaxel-CPP at the concentration of 100 M in aqueous solution (reprinted with permission from Ref. [56], © Elsevier B.V. 2015).

mean hydrodynamic diameter of CPP-paclitaxel nanospheres in aqueous media was 131.5 nm. The value obtained by DLS was slightly higher than the one obtained by TEM because the sample was dried for TEM observation [56].

### 3.2.3 Biological activity

The study of biological activity has been carried out on paclitaxel conjugated with a CPP (EEGRLYMRY-YSPTTRRYG). Half-inhibitory concentrations (IC<sub>50</sub>) were determined on human hepatocellular carcinoma cells (HepG2) by direct incubation of HepG2 cells with paclitaxel-CPP nanoparticles or free paclitaxel as a control. Then, evaluation of cell viability was carried out by the 1-(4,5-dimethylthiazol-2-yl)-3,5-diphenylformazan (MTT) assay. According to the results shown in Fig. 19, the paclitaxel-CPP nanospheres possessed slightly higher IC<sub>50</sub> values as compared to free paclitaxel against HepG2 cancer cells [56].

## 3.3 CPT-conjugated peptides

### 3.3.1 Preparation of amphiphilic compounds

CPT is an alkaloid that inhibits the nuclear enzyme type I DNA topoisomerase. This drug has shown anticancer activity but also low solubility in preliminary

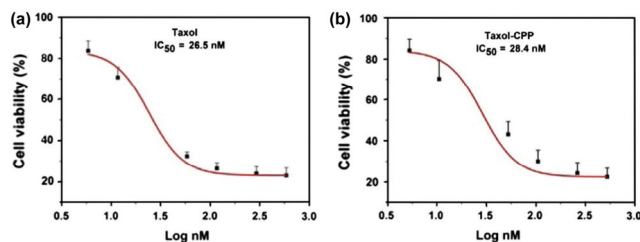


**Figure 19** Cytotoxicity of (a) free paclitaxel (Taxol) and (b) paclitaxel-CPP nanospheres against HepG2 cancer cells (reprinted with permission from Ref. [56], © Elsevier B.V. 2015).

clinical trials [58]. To alleviate this solubility problem, the anticancer drug was linked to a tripeptide, KCK (Lys-Cys-Lys), via a disulfide linkage [59]. To this end, the drug was functionalized with a pyridyl disulfide bond, and the conjugation was implemented via a thiol-disulfide exchange reaction. Practically, KCK was mixed with CPT at room temperature in dry dimethyl sulfoxide.

As for peptide-aliphatic chain conjugates, all the synthesis could be accomplished on a resin. For example, the tetrapeptide RGDS (Arg-Gly-Asp-Ser) was linked to a hydrophilic tail of tridecane ( $C_{13}H_{27}$ ) to obtain  $C_{13}H_{27}$ -CONH-Arg-Gly-Asp-Ser-Lys-COOH. This synthesis was carried out manually according to the Fmoc solid-phase peptide synthesis method. Then CPT-COOH was linked to the N terminus of lysine by the same coupling method [60].

### 3.3.2 Nanostructures formed by self-assembly

CPT is a hydrophobic drug needing a carrier to enhance the selectivity and cellular internalization. H. Choi et al. showed that it is possible to obtain different morphological features as a function of the prodrug concentration in aqueous media [61]. In fact, various self-assembled nanostructures of KCK-CPT have been observed by TEM: From nanotubes with a diameter of 100 nm at 800  $\mu$ M to nanosheets at 50  $\mu$ M (Fig. 20). Three main driving forces are responsible for the self-assembly: The hydrophilic-hydrophobic

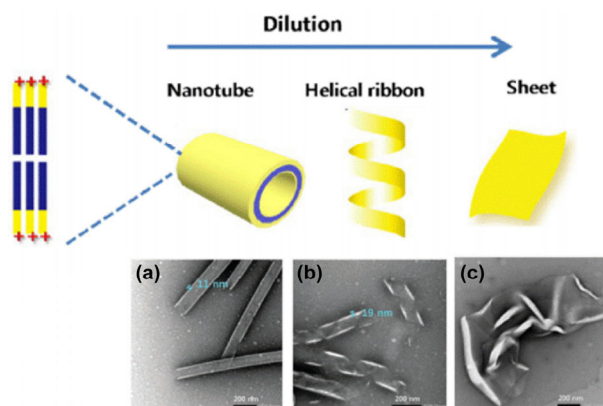


**Figure 20** Schematic representation of self-assembly of KCK-CPT conjugate and TEM images of self-assembled nanostructures obtained: (a) nanotube (width: 100 nm) formation at 800 mM in aqueous solution, (b) helical nanoribbon formation and (c) curved sheet nanostructure at 50  $\mu$ M in aqueous solution (adapted with permission from Ref. [59], © Royal Society of Chemistry 2016).

balance, intramolecular H-bonding, and aromatic  $\pi$ - $\pi$  interactions between the CPT units.

Nanofibers with a diameter of 20 nm can be obtained by self-assembly of RGD-CPT conjugates at 80  $\mu$ M [60]. Those authors investigated the self-assembly behavior of free peptides, to determine the participation of each driving force. According to previous results, the formation of nanofibers was mainly driven by the hydrophobic interaction and H-bonding [60].

### 3.3.3 Biological activity

CPT is linked to the tripeptide KCK through a disulfide bond that is cleavable in the intracellular reducing environment. Cellular uptake of the KCK-CPT conjugate has been analyzed in a mouse squamous carcinoma cell line, SCC-7 cells. CLSM experiments indicated rapid internalization of the conjugate by cells and that the nanostructure of the positively charged prodrug (KCK-CPT conjugate) had no selectivity for specific cancer cells. Accordingly, hyaluronic acid (HA) was complexed with the conjugate to improve the selectivity. HA is known as a tumor recognition moiety owing to its interaction with the cell surface receptor, CD44, abundant on most cancer cells [61]. HA is cleaved from HA-KCK-CPT via its degradation in endosomes and lysosomes by hyaluronidase. This change leads to the dissolution of the conjugate, while the positive charges of KCK-CPT allow for its release from the endosome [59].

In addition, biological activity of RGD-CPT has also been studied [60]. For this purpose, the drug release of CPT was investigated at pH 5.2 and 7.0. The results showed slow disassembly of nanofibers in both cases. On the other hand, the drug release rate was faster under acidic conditions owing to the accelerated cleavage of the succinyl linkage. Three cell lines were selected to study the *in vitro* toxicity: Mouse hepatoma H22 cells, human cervical carcinoma HeLa cells, and transformed African green monkey SV40-transformed kidney fibroblast (COS7) cells. According to cell viability assays, the presence of RGD in the prodrug promoted cellular uptake and enhanced cytotoxicity. To study the antitumor effect of the conjugate, those authors carried out *in vivo* studies in H22 tumor-bearing mice. For this purpose, RGD-prodrug was injected subcutaneously into mice.

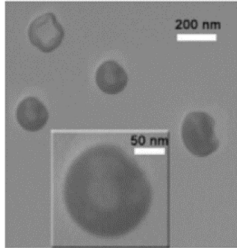
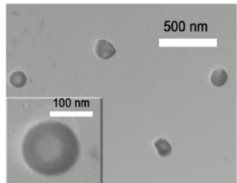
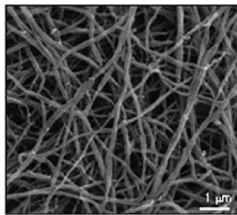
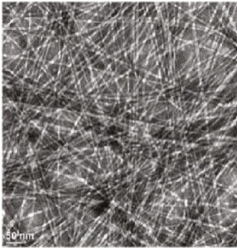
After 24 h, fluorescence intensity distribution revealed the presence of the prodrug not only in the tumor but also in the heart, liver, and kidney. The subcutaneously injected material first entered the lymphatic circulation system and then flowed through the body, which is why the prodrug could reach healthy organs. The *in vitro* and *in vivo* experiments indicated that this nanostructure may exert a substantial tumor suppression effect via the RGDS tetrapeptide with positive targeting

and nanoscale-assistant passive delivery [60].

## 4 Conclusion and perspectives

In summary, the self-assembly of peptide-based conjugates leads to a variety of nanostructures, among which micelles and nanofibers are the most common (Tables 1 and 2). These nanostructures are mainly obtained by pH-induced self-assembly in an aqueous

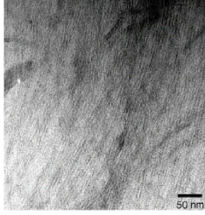
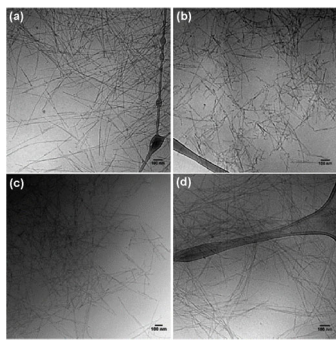
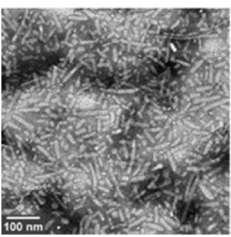
**Table 1** Different types of self-assembled aliphatic-chain conjugated peptides with biomedical application

Conjugates	Synthesis	Nanostructures	Modes of self-assembly	Targeted biomedical applications	Ref.
Aliphatic chain-conjugated peptides					
Disulfide bond linked stearyl-H <sub>3</sub> CR <sub>3</sub> C	SPPS	Doxorubicin-(DOX) and miR-34a-loaded cationic micelles ( $d = 169.8$ nm)	Probe-based ultrasonication technique	Prostate cancer (PC3 and DU145 cells)	[22]
					
		siRNA-loaded cationic micelles ( $d = 163$ nm)	Complexation with siRNA in PBS	Gene therapy Luciferase-expressing (GL3) HeLa cells (Luc-HeLa cells)	[23]
					
GS(P)E <sub>2</sub> L <sub>3</sub> A <sub>3</sub> -C <sub>16</sub> SDGRK <sub>2</sub> L <sub>3</sub> A <sub>3</sub> -C <sub>16</sub> GSE <sub>2</sub> L <sub>3</sub> A <sub>3</sub> -C <sub>16</sub> GAE <sub>2</sub> L <sub>3</sub> A <sub>3</sub> -C <sub>16</sub>	SPPS	Gels (networks of fibers $d = 30$ nm)	Gelation with metal cations: 40 mM aqueous PA solutions were mixed with 40 mM CaCl <sub>2</sub> (1:1 by volume)	Bone regeneration	[24]
					
C <sub>12</sub> -V <sub>2</sub> AGEGDK(pbs)S C <sub>12</sub> -V <sub>2</sub> AGL-NH <sub>2</sub> (Lys-PA)	SPPS	Gels (networks of fibers $d = 7.5$ nm)	Mixing PA with Ly-PA at 1:2 molar ratios	Tissue regeneration	[25]
					

(Continued)

Conjugates	Synthesis	Nanostructures	Modes of self-assembly	Targeted biomedical applications	Ref.
$C_{16}$ -A <sub>4</sub> G <sub>3</sub> -(KLAKLAK) <sub>2</sub>	SPPS	Nanotubes ( $d = 8\text{--}10$ nm, length = 100–900 nm)	Spontaneous self-assembly in phosphate buffer	Breast cancer (SKBR-3 and MDA-MB-231 cells)	[26]
Palmitoyl-p53 <sub>14-29</sub> p53 <sub>14-29</sub> :LSQETFSDLWK L <sub>2</sub> PEN	SPPS	Micelles ( $d = 319$ nm) and elongated micelles ( $d = 10$ nm, few hundred nanometers long)	Spontaneous self-assembly in phosphate buffer	Osteosarcoma	[28] [29]
CH <sub>3</sub> (CH <sub>2</sub> ) <sub>14</sub> CONH-GTAGLIGQ-RGDS CH <sub>3</sub> (CH <sub>2</sub> ) <sub>14</sub> CONH-GTAGLIGQ-DGEA CH <sub>3</sub> (CH <sub>2</sub> ) <sub>14</sub> CONH-GTAGLIGQ-KRSR CH <sub>3</sub> (CH <sub>2</sub> ) <sub>14</sub> CONH-GTAGLIGQ-RGES	SPPS	Cylindrical micelle nanofiber ( $d = 6\text{--}10$ nm, length dimension 50-fold greater)	Solution of PA in distilled water at pH 7.4. PA coating were dried at 37 °C for 2 days after evaporation of the solvent.	Bone tissue regeneration	[30]
DiC <sub>16</sub> -OVA <sub>253-266</sub> OVA <sub>253-266</sub> : EQLES <sub>2</sub> NFEKLTE	Peptide purchased on Rink amide. Dialkyl tails coupled to the N-terminal extremity before cleavage	Cylindrical micelles ( $d = 8$ nm, length = 50–300 nm)	PA dissolved in PBS at pH 9. The pH was then lowered to 7.4 using 0.1 N HCl in distilled water.	Antigen delivery system	[31]
C <sub>16</sub> -V <sub>2</sub> A <sub>2</sub> -K <sub>3</sub> G-KLTWQELYQLKYKGI-NH <sub>2</sub>	SPPS	Gels (network of fibers)	Gelation in water in the presence of divalent counterions	Therapy for ischemic cardiovascular disease	[32]
1,3-(dipalmitoyl)glycero-2-phosphoethanol-G <sub>2</sub> -HR1 <sub>Ala153-Gln202</sub>	SPPS	Star-like particles ( $d = 20$ nm)	Spontaneous self-assembly in phosphate buffer	Adjuvant-free stimulation of antigen specific humoral immune response	[33]

(Continued)

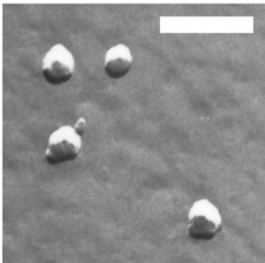
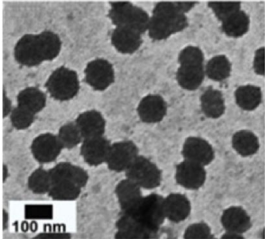
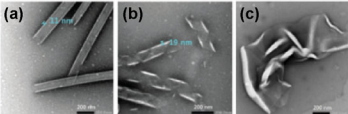
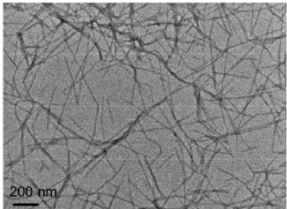
Conjugates	Synthesis	Nanostructures	Modes of self-assembly	Targeted biomedical applications	Ref.
Cholesterol-CH <sub>n</sub> R <sub>p</sub> with $n = 0, 3, 5$ and $p = 3, 5$	SPPS Conjugation through thiol-acrylate Michael type reaction	DNA-loaded cationic micelles. Size depends on the $N/P$ ratio (molar ratio of arginine residue ( $N$ ) in the peptide to phosphate group ( $P$ ) in the DNA molecule)	Mixing equal volume of cholesterol-peptide in PBS buffer (at 10 mg/mL) and DNA in nuclease-free water (at 1 mg/mL)	Gene delivery vectors MCF-7 (human breast adenocarcinoma) and HEK-293 cell lines	[34]
ARLPRK-pentynoyl-DPPE	SPPS and “click” chemistry (copper-catalysed alkyne-azide cycloaddition)	Membrane (height = 8 nm)	The lipid monolayer of peptide-conjugated lipid was loaded onto POPC(1-palmitoyl-2-oleoyl-sn-glycero-3-phosphocholine)-coated mica	Detection of Hemagglutinin	[35]
DSPE-PEG <sub>2000</sub> -(FAM)-CREKA	SPPS then DSPE-PEG <sub>2000</sub> -maleimide linked to the cysteine via a thioether linkage	Micelles ( $d = 17$ nm)	Spontaneous self-assembly in aqueous solution	Cardiovascular disease	[36]
Alkyl-A <sub>4</sub> G <sub>3</sub> S <sup>(P)</sup> RGD-COOH	SPPS	Gels (networks of fibers $d = 5-6$ nm) 	Gelation with metal cations: 10 mM aqueous conjugate solutions were mixed with cations	Cell transplantation or other tissue engineering applications	[38]
C <sub>16</sub> -V <sub>2</sub> A <sub>2</sub> E <sub>2</sub> K-Hyd-Prodan	Synthesis of peptide containing hydrazide via SPPS Condensation of Prodan	Gels (cross sectional diameter = 10–11 nm) 	Gelation in presence of divalent counterions: PA dissolved in 10 mM NaOH were mixed with a solution of 100 mM CaCl <sub>2</sub>	Controlled release of small molecules (Prodan)	[39]
diC <sub>16</sub> -J <sub>8</sub>	SPPS diC <sub>16</sub> coupled to the N-terminal extremity of peptide by an amidation reaction	Micelles ( $d = 5-15$ nm, length = 25–125 nm) 	PA were film cast by mehtnaol evaporation and rehydrated to allow micelle formation	Vaccine that protect against GAS	[41]



(Continued)

Conjugates	Synthesis	Nanostructures	Modes of self-assembly	Targeted biomedical applications	Ref.
(C <sub>18</sub> ) <sub>2</sub> -E-C <sub>2</sub> -RGD RGD-C <sub>2</sub> -E-(C <sub>18</sub> ) <sub>2</sub> (C <sub>18</sub> ) <sub>2</sub> -E-C <sub>2</sub> -RGD-C <sub>2</sub> -E-(C <sub>18</sub> ) <sub>2</sub>	Solution-phase-peptide synthesis then dialkyl tail linked to the peptide	Monolayers	Langmuir-Blodgett film deposition with control of surface pressure	Biomimetic coatings	[44]

**Table 2** Different types of self-assembled drug-conjugated peptides with biomedical application

Conjugates	Synthesis	Nanostructures	Modes of self-assembly	Targeted biomedical applications	Ref.
Drug-conjugated peptides					
DOX-ELP	ELP[V <sub>5</sub> A <sub>2</sub> G <sub>3</sub> -150] ELP[V <sub>1</sub> A <sub>8</sub> G <sub>7</sub> -160]	Recombinant synthesis and thiol-maleimide “click” chemistry	Micelles below its first transition ( <i>R<sub>h</sub></i> = 21 nm) and a terminal aggregate after its transition	Squamous cell carcinoma (FaDu)	[47]
DOX-CP CP: Chimeric Polypeptide	ELP:SKGPG-ELP [(VPGXG) <sub>10</sub> ] <sub>18</sub> -WPC with X = V, A and G residues with 5:2:3 ratio	Recombinant synthesis and thiol-maleimide “click” chemistry	Micelles ( <i>d</i> = 40 nm)	Temperature-dependent self-assembly in PBS	Colon carcinoma (C26 murine cells)
	Recombinant synthesis and thiol-maleimide “click” chemistry				T1-luciferase murine mammary carcinoma cells Lewis lung carcinoma LL/2-Luc-M38 (LLC) cells
Paclitaxel-CPP CPP: Cell-Penetrating Peptide	CPP: E <sub>2</sub> GRLYMRY <sub>2</sub> SPT <sub>2</sub> R <sub>2</sub> YG	SPPS and carbodiimide-mediated coupling reaction	Nanospheres ( <i>d</i> = 120 nm)	Spontaneous self-assembly in distilled water of phosphate buffer saline (pH 7.4)	Liver hepatocellular carcinoma (HepG2 cells)
					[56]
			Morphologies from nanotubes to nanosheets depends on the concentration.		
KCK			(a) 800 mM (b) 50 mM (c) 50 mM	Spontaneous self-assembly in water	Squamous carcinoma (SCC-7 cells)
					[59]
Camptothecin-peptide		SPPS and thiol-disulfide exchange reaction	Nanofibers ( <i>d</i> = 20 nm)	Spontaneous self-assembly in PBS (concentration of 10 mM)	Tumorous H22, HeLa cells, and normal COS-7 cells
	RGDS				[60]

solution, but it is also possible to employ a divalent-ion induction process or a probe-based ultrasonication technique to load a drug into the core of the micelles. Concerning the properties of the resultant nanostructures and their biological activity, there are more studies on aliphatic-chain-conjugated peptides than on drug-conjugated peptides. Peptide-based conjugates are an emerging research area. Nevertheless, as shown in Table 2, conjugation of a peptide with a drug to form an amphiphilic conjugate with a potent biological activity has not been explored much. This is true for ferrocene-based molecules, which have antiproliferative effects and reversible redox properties [62, 63]. In fact, B. Adhikari et al. have studied the gel formation of different conjugates containing ferrocenecarboxylic acid or ferrocenylacrylic acid without providing guidance on biological activity [64]. On the other hand, an *in vitro* study was conducted on ferrocenecarboxylic acid conjugated with polyarginine (hexa- or octa-arginine) without a relation between the results obtained and potential formation of nanostructures [65].

In the future, three strategies can help to vectorize a drug: A combination of CPPs, prodrug, and nanoparticle technologies (Fig. 21).

The use of CPPs as building blocks has significant advantages in nanomedical applications because of their biocompatibility, responsiveness to environmental changes, and the ability to facilitate cellular uptake. The coupling of a hydrophilic CPP with a hydrophobic drug should inactivate the drug and enable the release mostly in cancer cells. To this end, the drug may be linked to a CPP via a biocleavable bond, ideally cleavable by enzymes expressed in the intracellular environment of cancer cells. Therefore, this alternative strategy, derived from the prodrug concept, may limit the burst release [66] and allow for an increase in drug loading. Moreover, the choice of the CPP will be crucial to attain specific targeting, and some CPPs are

known to be specific for cancerous cells, such as the TLS peptide for ovarian cancer cells, and RLW for lung cancer cells [67, 68].

## References

- [1] Bangham, A. D.; Standish, M. M.; Watkins, J. C. Diffusion of univalent ions across the lamellae of swollen phospholipids. *J. Mol. Biol.* **1965**, *13*, 238–252.
- [2] Allen, T. M.; Cullis, P. R. Liposomal drug delivery systems: From concept to clinical applications. *Adv. Drug Deliv. Rev.* **2013**, *65*, 36–48.
- [3] Croy, S. R.; Kwon, G. S. Polymeric micelles for drug delivery. *Curr. Pharm. Des.* **2006**, *12*, 4669–4684.
- [4] Mandal, A.; Bisht, R.; Rupenthal, I. D.; Mitra, A. K. Polymeric micelles for ocular drug delivery: From structural frameworks to recent preclinical studies. *J. Control. Release* **2017**, *248*, 96–116.
- [5] Panahi, Y.; Farshbaf, M.; Mohammadhosseini, M.; Mirahadi, M.; Khalilov, R.; Saghfi, S.; Akbarzadeh, A. Recent advances on liposomal nanoparticles: Synthesis, characterization and biomedical applications. *Artif. Cells Nanomed. Biotechnol.* **2017**, *45*, 788–799.
- [6] Mehrabi, M.; Esmailpour, P.; Akbarzadeh, A.; Saffari, Z.; Farahnak, M.; Farhangi, A.; Chiani, M. Efficacy of PEGylated liposomal etoposide nanoparticles on breast cancer cell lines. *Turk. J. Med. Sci.* **2016**, *46*, 567–571.
- [7] Vahed Zununi, S.; Salehi, R.; Davaran, S.; Sharifi, S. Liposome-based drug co-delivery systems in cancer cells. *Mater. Sci. Eng. C* **2017**, *71*, 1327–1341.
- [8] Venev, S. V.; Reineker, P.; Potemkin, I. I. Direct and inverse micelles of diblock copolymers with a polyelectrolyte block: Effect of equilibrium distribution of counterions. *Macromolecules* **2010**, *43*, 10735–10742.
- [9] Gennes, P. G. *Scaling Concepts in Polymer Physics*; Cornell University Press: Ithaca, NY, 1979.
- [10] Birshtein, T. M.; Zhulina, E. B. Scaling theory of supermolecular structures in block copolymer-solvent systems: 1. Model of micellar structures. *Polymer* **1989**, *30*, 170–177.
- [11] Jain, S.; Bates, F. S. On the origins of morphological complexity in block copolymer surfactants. *Science* **2003**, *300*, 460–464.
- [12] Israelachvili, J. N.; Mitchell, D. J.; Ninham, B. W. Theory of self-assembly of hydrocarbon amphiphiles into micelles and bilayers. *J. Chem. Soc. Faraday Trans. 2* **1976**, *72*, 1525–1568.
- [13] Israelachvili, J. N. Thermodynamic and geometric aspects



**Figure 21** Scheme of the synthesis of prodrug nanoparticles.

- of amphiphile aggregation into micelles, vesicles and bilayers and the interactions between them. In *Physics of Amphiphiles: Micelles, Vesicles and Microemulsions: Proceedings of the International School of Physics, Enrico Fermi, Course Xc*. Degiorgio, V.; Corti, M., Eds.; Elsevier Science Ltd: Amsterdam, 1985; pp 24–58.
- [14] Israelachvili, J. N. 20-Soft and biological structures. In *Intermolecular and Surface Forces*. 3rd Ed. Israelachvili, J. N., Ed.; Academic Press: San Diego, 2011; pp 535–576.
- [15] Holmberg, K.; Jönsson, B.; Kronberg, B.; Lindman, B. Front matter. In *Surfactants and Polymers in Aqueous Solution*. 2nd ed. Holmberg, K.; Jönsson, B.; Kronberg, B.; Lindman, B., Eds.; John Wiley & Sons, Ltd: Chichester, 2003.
- [16] Lepeltier, E.; Bourgaux, C.; Maksimenko, A.; Meneau, E.; Rosilio, V.; Sliwinski, E.; Zouhiri, F.; Desmaële, D.; Couvreur, P. Self-assembly of polyisoprenoyl gemcitabine conjugates: Influence of supramolecular organization on their biological activity. *Langmuir* **2014**, *30*, 6348–6357.
- [17] Naik, S. S.; Savin, D. A. Poly(Z-lysine)-based organogels: Effect of interfacial frustration on gel strength. *Macromolecules* **2009**, *42*, 7114–7121.
- [18] Nowak, A. P.; Breedveld, V.; Pakstis, L.; Ozbas, B.; Pine, D. J.; Pochan, D.; Deming, T. J. Rapidly recovering hydrogel scaffolds from self-assembling diblock copolypeptide amphiphiles. *Nature* **2002**, *417*, 424–428.
- [19] Holowka, E. P.; Pochan, D. J.; Deming, T. J. Charged polypeptide vesicles with controllable diameter. *J. Am. Chem. Soc.* **2005**, *127*, 12423–12428.
- [20] Denisov, I. G.; Grinkova, Y. V.; Lazarides, A. A.; Sligar, S. G. Directed self-assembly of monodisperse phospholipid bilayer nanodiscs with controlled size. *J. Am. Chem. Soc.* **2004**, *126*, 3477–3487.
- [21] Sigg, S. J.; Postupalenko, V.; Duskey, J. T.; Palivan, C. G.; Meier, W. Stimuli-responsive codelivery of oligonucleotides and drugs by self-assembled peptide nanoparticles. *Biomacromolecules* **2016**, *17*, 935–945.
- [22] Yao, C.; Liu, J. Y.; Wu, X.; Tao, Z. G.; Gao, Y.; Zhu, Q. G.; Li, J. F.; Zhang, L. J.; Hu, C. L.; Gu, F. F. et al. Reducible self-assembling cationic polypeptide-based micelles mediate co-delivery of doxorubicin and microRNA-34a for androgen-independent prostate cancer therapy. *J. Control. Release* **2016**, *232*, 203–214.
- [23] Tai, Z. G.; Wang, X. Y.; Tian, J.; Gao, Y.; Zhang, L. J.; Yao, C.; Wu, X.; Zhang, W.; Zhu, Q. G.; Gao, S. Biodegradable stearylated peptide with internal disulfide bonds for efficient delivery of siRNA *in vitro* and *in vivo*. *Biomacromolecules* **2015**, *16*, 1119–1130.
- [24] Hartgerink, J. D.; Beniash, E.; Stupp, S. I. Peptide-amphiphile nanofibers: A versatile scaffold for the preparation of self-assembling materials. *Proc. Natl. Acad. Sci. USA* **2002**, *99*, 5133–5138.
- [25] Mata, A.; Geng, Y. B.; Henrikson, K. J.; Aparicio, C.; Stock, S. R.; Satcher, R. L.; Stupp, S. I. Bone regeneration mediated by biomimetic mineralization of a nanofiber matrix. *Biomaterials* **2010**, *31*, 6004–6012.
- [26] Mammadov, R.; Mammadov, B.; Toksoz, S.; Aydin, B.; Yagci, R.; Tekinay, A. B.; Guler, M. O. Heparin mimetic peptide nanofibers promote angiogenesis. *Biomacromolecules* **2011**, *12*, 3508–3519.
- [27] Standley, S. M.; Toft, D. J.; Cheng, H.; Soukasene, S.; Chen, J.; Raja, S. M.; Band, V.; Band, H.; Cryns, V. L.; Stupp, S. I. Induction of cancer cell death by self-assembling nanostructures incorporating a cytotoxic peptide. *Cancer Res.* **2010**, *70*, 3020–3026.
- [28] Missirlis, D.; Krogstad, D. V.; Tirrell, M. Internalization of p53<sub>14-29</sub> peptide amphiphiles and subsequent endosomal disruption results in SJS-1 cell death. *Mol. Pharmaceutics* **2010**, *7*, 2173–2184.
- [29] Missirlis, D.; Khant, H.; Tirrell, M. Mechanisms of peptide amphiphile internalization by SJS-1 cells *in vitro*. *Biochemistry* **2009**, *48*, 3304–3314.
- [30] Anderson, J. M.; Kushwaha, M.; Tambralli, A.; Bellis, S. L.; Camata, R. P.; Jun, H. W. Osteogenic differentiation of human mesenchymal stem cells directed by extracellular matrix-mimicking ligands in a biomimetic self-assembled peptide amphiphile nanomatrix. *Biomacromolecules* **2009**, *10*, 2935–2944.
- [31] Black, M.; Trent, A.; Kostenko, Y.; Lee, J. S.; Olive, C.; Tirrell, M. Self-assembled peptide amphiphile micelles containing a cytotoxic t-cell epitope promote a protective immune response *in vivo*. *Adv. Mater.* **2012**, *24*, 3845–3849.
- [32] Webber, M. J.; Tongers, J.; Newcomb, C. J.; Marquardt, K. T.; Bauersachs, J.; Losordo, D. W.; Stupp, S. I. Supramolecular nanostructures that mimic VEGF as a strategy for ischemic tissue repair. *Proc. Natl. Acad. Sci. USA* **2011**, *108*, 13438–13443.
- [33] Boato, F.; Thomas, R. M.; Ghasparian, A.; Freund-Renard, A.; Moehle, K.; Robinson, J. A. Synthetic virus-like particles from self-assembling coiled-coil lipopeptides and their use in antigen display to the immune system. *Angew. Chem., Int. Ed.* **2007**, *46*, 9015–9018.
- [34] Tang, Q.; Cao, B.; Wu, H. Y.; Cheng, G. Cholesterol-peptide hybrids to form liposome-like vesicles for gene delivery. *PLoS One* **2013**, *8*, e54460.

- [35] Matsubara, T.; Shibata, R.; Sato, T. Binding of hemagglutinin and influenza virus to a peptide-conjugated lipid membrane. *Front. Microbiol.* **2016**, *7*, 468.
- [36] Peters, D.; Kastantin, M.; Kotamraju, V. R.; Karmali, P. P.; Gujrati, K.; Tirrell, M.; Ruoslahti, E. Targeting atherosclerosis by using modular, multifunctional micelles. *Proc. Natl. Acad. Sci. USA* **2009**, *106*, 9815–9819.
- [37] Tornøe, C. W.; Christensen, C.; Meldal, M. Peptidotriazoles on solid phase: [1,2,3]-triazoles by regioselective copper(I)-catalyzed 1,3-dipolar cycloadditions of terminal alkynes to azides. *J. Org. Chem.* **2002**, *67*, 3057–3064.
- [38] Beniash, E.; Hartgerink, J. D.; Storrer, H.; Stendahl, J. C.; Stupp, S. I. Self-assembling peptide amphiphile nanofiber matrices for cell entrapment. *Acta Biomater.* **2005**, *1*, 387–397.
- [39] Matson, J. B.; Newcomb, C. J.; Bitton, R.; Stupp, S. I. Nanostructure-templated control of drug release from peptide amphiphile nanofiber gels. *Soft Matter* **2012**, *8*, 3586–3595.
- [40] Cui, H. G.; Muraoka, T.; Cheetham, A. G.; Stupp, S. I. Self-assembly of giant peptide nanobelts. *Nano Lett.* **2009**, *9*, 945–951.
- [41] Trent, A.; Ulery, B. D.; Black, M. J.; Barrett, J. C.; Liang, S. M.; Kostenko, Y.; David, N. A.; Tirrell, M. V. Peptide amphiphile micelles self-adjuvant group a streptococcal vaccination. *AAPS J.* **2015**, *17*, 380–388.
- [42] Matsubara, T.; Iijima, K.; Yamamoto, N.; Yanagisawa, K.; Sato, T. Density of GM1 in nanoclusters is a critical factor in the formation of a spherical assembly of amyloid  $\beta$ -protein on synaptic plasma membranes. *Langmuir* **2013**, *29*, 2258–2264.
- [43] Iijima, K.; Soga, N.; Matsubara, T.; Sato, T. Observations of the distribution of GM3 in membrane microdomains by atomic force microscopy. *J. Colloid Interface Sci.* **2009**, *337*, 369–374.
- [44] Pakalns, T.; Haverstick, K. L.; Fields, G. B.; McCarthy, J. B.; Mooradian, D. L.; Tirrell, M. Cellular recognition of synthetic peptide amphiphiles in self-assembled monolayer films. *Biomaterials* **1999**, *20*, 2265–2279.
- [45] Ma, W.; Cheetham, A. G.; Cui, H. G. Building nanostructures with drugs. *Nano Today* **2016**, *11*, 13–30.
- [46] Gewirtz, D. A critical evaluation of the mechanisms of action proposed for the antitumor effects of the anthracycline antibiotics adriamycin and daunorubicin. *Biochem. Pharmacol.* **1999**, *57*, 727–741.
- [47] Dreher, M. R.; Raucher, D.; Balu, N.; Colvin Michael, O.; Ludeman, S. M.; Chilkoti, A. Evaluation of an elastin-like polypeptide-doxorubicin conjugate for cancer therapy. *J. Control. Release* **2003**, *91*, 31–43.
- [48] Furgeson, D. Y.; Dreher, M. R.; Chilkoti, A. Structural optimization of a ‘smart’ doxorubicin–polypeptide conjugate for thermally targeted delivery to solid tumors. *J. Control. Release* **2006**, *110*, 362–369.
- [49] MacKay, A. J.; Chen, M. N.; McDaniel, J. R.; Liu, W. G.; Simnick, A. J.; Chilkoti, A. Self-assembling chimeric polypeptide–doxorubicin conjugate nanoparticles that abolish tumours after a single injection. *Nat. Mater.* **2009**, *8*, 993–999.
- [50] Mastria, E. M.; Chen, M. N.; McDaniel, J. R.; Li, X. H.; Hyun, J.; Dewhirst, M. W.; Chilkoti, A. Doxorubicin-conjugated polypeptide nanoparticles inhibit metastasis in two murine models of carcinoma. *J. Control. Release* **2015**, *208*, 52–58.
- [51] Cheng, H.; Zhu, J. Y.; Xu, X. D.; Qiu, W. X.; Lei, Q.; Han, K.; Cheng, Y. J.; Zhang, X. Z. Activable cell-penetrating peptide conjugated prodrug for tumor targeted drug delivery. *Appl. Mater. Interfaces* **2015**, *7*, 16061–16069.
- [52] Shi, N. Q.; Gao, W.; Xiang, B.; Qi, X. R. Enhancing cellular uptake of activable cellpenetrating peptide–doxorubicin conjugate by enzymatic cleavage. *Int. J. Nanomedicine* **2012**, *7*, 1613–1621.
- [53] Yang, Y. F.; Yang, Y.; Xie, X. Y.; Cai, X.S.; Zhang, H.; Gong, W.; Wang, Z. Y.; Mei, X. G. PEGylated liposomes with NGR ligand and heat-activable cell penetrating peptide-doxorubicin conjugate for tumor-specific therapy. *Biomaterials* **2014**, *35*, 4368–4381.
- [54] Liang, J. F.; Yang, V. C. Synthesis of doxorubicin-peptide conjugate with multidrug resistant tumor cell killing activity. *Bioorg. Med. Chem. Lett.* **2005**, *15*, 5071–5075.
- [55] Wani, M. C.; Taylor, H. L.; Wall, M. E.; Coggon, P.; McPhail, A. T. Plant antitumor agents. VI. Isolation and structure of taxol, a novel antileukemic and antitumor agent from *Taxus brevifolia*. *J. Am. Chem. Soc.* **1971**, *93*, 2325–2327.
- [56] Tian, R.; Wang, H. M.; Niu, R. F.; Ding, D. Drug delivery with nanospherical supramolecular cell penetrating peptide-taxol conjugates containing a high drug loading. *J. Colloid Interface Sci.* **2015**, *453*, 15–20.
- [57] Dubikovskaya, E. A.; Thorne, S. H.; Pillow, T. H.; Contag, C. H.; Wender, P. A. Overcoming multidrug resistance of small-molecule therapeutics through conjugation with releasable octaarginine transporters. *Proc. Natl. Acad. Sci. USA* **2008**, *105*, 12128–12133.
- [58] Thomas, C. J.; Rahier, N. J.; Hecht, S. M. Camptothecin: Current perspectives. *Bioorg. Med. Chem.* **2004**, *12*, 1585–1604.
- [59] Choi, H.; Jeena, M. T.; Palanikumar, L.; Jeong, Y.; Park, S.;

- Lee, E.; Ryu, J. H. The HA-incorporated nanostructure of a peptide–drug amphiphile for targeted anticancer drug delivery. *Chem. Commun.* **2016**, *52*, 5637–5640.
- [60] Peng, M. Y.; Qin, S. Y.; Jia, H. Z.; Zheng, D. W.; Rong, L.; Zhang, X. Z. Self-delivery of a peptide based prodrug for tumor-targeting therapy. *Nano Res.* **2015**, *9*, 663–673.
- [61] Ossipov, D. A. Nanostructured hyaluronic acid-based materials for active delivery to cancer. *Expert Opinion Drug Deliv.* **2010**, *7*, 681–703.
- [62] Fish, R. H.; Jaouen, G. Bioorganometallic chemistry: Structural diversity of organometallic complexes with bioligands and molecular recognition studies of several supramolecular hosts with biomolecules, alkali-metal ions, and organometallic pharmaceuticals. *Organometallics* **2003**, *22*, 2166–2177.
- [63] Fouda, M. F. R.; Abd-Elzaher, M. M.; Abdelsamaia, R. A.; Labib, A. A. On the medicinal chemistry of ferrocene. *Appl. Organomet. Chem.* **2007**, *21*, 613–625.
- [64] Adhikari, B.; Singh, C.; Shah, A.; Lough, A. J.; Kraatz, H. B. Amino acid chirality and ferrocene conformation guided self-assembly and gelation of ferrocene-peptide conjugates. *Chem.-Eur. J.* **2015**, *21*, 11560–11572.
- [65] Miklán, Z.; Szabó, R.; Zsoldos-Mády, V.; Reményi, J.; Bánóczy, Z.; Hudecz, F. New ferrocene containing peptide conjugates: Synthesis and effect on human leukemia (HL-60) cells. *Biopolymers* **2007**, *88*, 108–114.
- [66] Huang, X.; Brazel, C. S. On the importance and mechanisms of burst release in matrix-controlled drug delivery systems. *J. Control. Release* **2001**, *73*, 121–136.
- [67] Ma, C. Y.; Yin, G. F.; You, F.; Wei, Y.; Huang, Z. B.; Chen, X. C.; Yan, D. H. A specific cell-penetrating peptide induces apoptosis in SKOV3 cells by down-regulation of Bcl-2. *Biotechnol. Lett.* **2013**, *35*, 1791–1797.
- [68] Gao, H. L.; Zhang, Q. Y.; Yang, Y. T.; Jiang, X. G.; He, Q. Tumor homing cell penetrating peptide decorated nanoparticles used for enhancing tumor targeting delivery and therapy. *Int. J. Pharm.* **2015**, *478*, 240–250.